Acta Oceanol. Sin., 2019, Vol. 38, No. 8, P. 101–110
https://doi.org/10.1007/s13131-019-1451-1
http://www.hyxb.org.cn
E-mail: hyxbe@263.net

Changes in sea ice kinematics in the Arctic outflow region and their associations with Arctic Northeast Passage accessibility

Dawei Gui[1, 2], Xiaoping Pang[1], Ruibo Lei[2, 1*], Xi Zhao[1], Jia Wang[3]

[1] Chinese Antarctic Center of Surveying and Mapping, Wuhan University, Wuhan 430079, China

[2] MNR Key Laboratory for Polar Science, Polar Research Institute of China, Shanghai 200136, China

[3] National Oceanic and Atmospheric Administration Great Lakes Environmental Research Laboratory, Ann Arbor 48108-9719, USA

Received 6 June 2018; accepted 10 September 2018

© Chinese Society for Oceanography and Springer-Verlag GmbH Germany, part of Springer Nature 2019

Abstract

Amplification of climate warming in the Arctic is causing a dramatic retreat of sea ice, which means the Arctic sea routes are becoming increasingly accessible. This study used a satellite-derived sea ice motion product to quantify the kinematic features of sea ice in the Arctic outflow region which specially referred to the Fram Strait and to the north of the Northeast Passage (NEP). An observed trend of increased southward sea ice displacement from the central Arctic to the Fram Strait indicated enhancement of the Transpolar Drift Stream (TDS). In the regions to the north of the NEP, the long-term trend of northward sea ice speed in the Kara sector was +0.04 cm/s per year in spring. A significant statistical relationship was found between the NEP open period and the northward speed of the sea ice to the north of the NEP. The offshore advection of sea ice could account for the opening of sea routes by 33% and 15% in the Kara and Laptev sectors, respectively. The difference in sea level pressure across the TDS, i.e., the Central Arctic Index (CAI), presented more significant correlation than for the Arctic atmospheric Dipole Anomaly index with the open period of the NEP, and the CAI could explain the southward displacement of sea ice toward the Fram Strait by more than 45%. The impact from the summer positive CAI reinforces the thinning and mechanical weakening of the sea ice in the NEP region, which improves the navigability of the NEP.

Key words: sea ice, Arctic Northeast Passage, Transpolar Drift Stream, atmospheric circulation indices

Citation: Gui Dawei, Pang Xiaoping, Lei Ruibo, Zhao Xi, Wang Jia. 2019. Changes in sea ice kinematics in the Arctic outflow region and their associations with Arctic Northeast Passage accessibility. Acta Oceanologica Sinica, 38(8): 101–110, doi: 10.1007/s13131-019-1451-1

1 Introduction

Increasing amounts of evidence have proven Arctic sea ice is undergoing remarkable loss. Satellite-derived data have revealed that the overall extent and area of sea ice have shown significant trends of decline since 1979 (Comiso and Hall, 2014). The trend in annual mean ice thickness over the Arctic Basin was –(0.58± 0.07) m per decade during 2000–2012 (Lindsay and Schweiger, 2015). The thinning of ice thickness has been caused mainly by the retreat of the perennial ice, which can induce further mechanical weakening. In this thinning process, sea ice can become more mobile, fractured, and deformed without an increase in the wind speed (Spreen et al., 2011). It has been reported that the spatially averaged trend in ice drift speed over the Arctic Basin increased between 2001 and 2009 by +23.6% per decade in winter and +17.7 % per decade in summer (Kwok et al., 2013)

Reduction of sea ice potentially facilitates the accessibility of Arctic sea routes. The sea route between Europe and Asia could be shortened substantially via passage through the Arctic Ocean (Lasserre and Pelletier, 2011). Recently, sea ice conditions along the Northeast Passage (NEP) have changed substantially with both the concentration and the thickness of ice showing trends of decline, which have led to improved accessibility in recent years. The length of the NEP open period, defined with a threshold of ice concentration less than 50%, has increased from 84 d in the 1980s to 114 d in the 2000s, and it even reached 146 d in 2012 (Lei et al., 2015). Across the Eastern Siberian Shelf, including the Laptev Sea and East Siberian Sea, sea ice conditions have a close relationship with Siberian river runoff, and coastal polynya events (Dmitrenko et al., 2005, 2008). The offshore components of surface wind forcing can increase the activities of coastal polynyas which result in an extension of the summer melt period (Bareiss and Görgen, 2005; Dmitrenko et al., 2009). Consequently, coastal polynya activities might have a connection with the sea ice condition along the NEP in summer. Most parts of the Arctic NEP are located in the upstream region of the Transpolar Drift Stream (TDS). The enhanced TDS can strengthen the export of sea ice from the central Arctic region to lower latitudes, which is closely related to the reduction of Arctic sea ice extent (Nghiem et al., 2007) and could likely lead to the opening of NEP.

The response of sea ice to the variability of atmospheric circulation patterns, especially the North Atlantic Oscillation (NAO) and the Arctic Oscillation (AO), has been investigated in many studies (Hurrell, 1995; Thompson and Wallace, 1998; Kwok and Rothrock, 1999; Wang and Ikeda, 2000; Rigor et al., 2002; Zhang et al., 2003). However, the relationship of the Arctic atmospheric Dipole Anomaly (DA) with sea ice motion along the TDS has been revealed more significant than that of either the NAO or the

Foundation item: The National Key Research and Development Program of China under contract Nos 2018YFA0605903 and 2016YFC14003; the National Natural Science Foundation of China under contract No. 41722605.
*Corresponding author, E-mail: leiruibo@pric.org.cn

AO, because the DA is associated with the high- and low-pressure centers across the TDS (Wu et al., 2006; Wang et al., 2009). During 1979–2011, the mean travel time from 88°N to 80°N in the section 60°W–60°E was 183(±29) d, and about 31% of the variation in ice travel time could be explained by monthly DA index (Lei et al., 2016). The Central Arctic Index (CAI) is defined as the sea level pressure (SLP) difference across the Arctic Ocean along the meridians of 90°W and 90°E. Based on analysis of atmospheric forcing on the drift of Arctic sea ice in 1989–2009, Vihma et al. (2012) found the CAI had stronger correlation than the DA index with the Arctic sea ice outflow through the TDS, because the locations of the high- and low-pressure centers of the DA have considerable interannual variability.

The characteristics of both the sea ice conditions and the NEP open period in relation to the DA index have already been investigated in a previous study (Lei et al., 2015). However, the kinematic characteristics of sea ice to the north of the NEP, which might be closely related to the open period, have not been evaluated, and the relationship between the TDS and the NEP open period has yet to be verified using observational data. This study focused on the condition of sea ice motion in the Arctic outflow region which specially referred to the Fram Strait and to the north of the NEP. Using a satellite-derived motion product, the objective was to investigate the response of ice motion to the atmospheric circulation patterns and to establish a relationship with the NEP accessibility. The results could support improving the predictability of the NEP open period, which is very important for the planning processes of the related stakeholders, e.g., ship owners, insurance agents, and navigation authorities.

2 Data and methods

2.1 *Satellite-derived products and buoy data of sea ice motion*

In comparison with buoy data, satellite-derived ice motion products can provide continuous and large-scale observations. The National Snow and Ice Data Center (NSIDC) ice drift velocity dataset (Version 3 available from www.nsidc.org), derived from a wide variety of sensors, is available with daily temporal resolution and 25-km spatial resolution (Table 1). The correlation coefficients between the NSIDC data and buoy data are 0.94 in winter and 0.87 in summer and the root mean square errors are 1.0 cm/s in winter and 1.3 cm/s in summer (Sumata et al., 2014). Given its acceptable accuracy and long-term coverage (1978 to present), we used the NSIDC dataset to calculate the southward sea ice displacement in the Arctic outflow region and the northward sea ice speed to the north of the NEP during 1979–2014 (except for 1993 because of a data gap). We focused on these two kinematic parameters of sea ice because they probably have potential relationships with the NEP accessibility.

Table 1. Description of remote sensing data used in this study

Product	Data source	Period	Spatial resolution	Temporal resolution	Reference
Ice motion	NSIDC	1979–2014	25 km	1 d	Tschudi et al. (2016)
	OSI SAF	2006–2014 (only available in freezing season)	62.5 km	2 d	OSI SAF, www.osi-saf.org
Ice concentration	SMMR	1979–1986	25 km	2 d	Cavalieri et al. (1996)
	SSM/I	1987–2007	25 km	1 d	Cavalieri et al. (1996)
	SSMIS	2008–2014	25 km	1 d	Cavalieri et al. (1996)

In-situ data measured by five ice-tethered buoys from October 2011 to April 2012, and the Ocean and Sea Ice Satellite Application Facility (OSI SAF) ice velocity product (available from www.osi-saf.org) for 2006–2014 were used to validate the NISDC product. The OSI SAF ice velocity product is retrieved from aggregated maps of passive microwave and scatterometer sensors (Lavergne et al., 2010). Because of the uselessness of information in summer when the ice surface is melting, the OSI SAF product with 62.5-km spatial resolution and 2-d temporal resolution is available only during October–April. The buoy data used here were acquired by the following instruments: two Ice-Tethered Profilers (ITP58 and ITP60) deployed at 82.91°N, 109.82°E on August 21, 2012 and at 85.06°N, 122.71°E on September 8, 2012, respectively, by the Hybrid Arctic/Antarctic Float Observation System (HAFOS), one MetOcean Ice-Mass Balance (IMB) buoy (2012J_IMB) deployed at 82.88°N, 130.06°E on August 25, 2012 by the German Arctic cruise, and two Snow and Ice Mass Balance Array buoys (SIMBA a and SIMBA b), which were deployed at 85.04°N, 145.99°E on September 2, 2012, and at 85.16°N, 123.09°E on September 7, 2012, respectively, by the Chinese National Arctic Research Expedition. The positions were measured every 2 h by the SIMABAs, while the data from the other buoys had 1-h temporal resolution. The positioning accuracy of all buoys is better than 15 m. The NSIDC and OSI SAF ice drift velocity datasets were used to reconstruct the Lagrangian trajectories of the sea ice from the deployment sites of the buoys. Then, we calculated the ice drift speed along the trajectories, and estimated the deviation between the remote sensing products and the buoy data to assess the data quality of the former.

The transport time of ice from the central Arctic Ocean to the Fram Strait can indicate the strength of the TDS. Thus, we defined three start sites at 88°N (black dots labeling as A1–A3 in Fig. 1) to estimate the transport time from the central Arctic Ocean toward the Fram Strait in accordance with Lei et al. (2016). The longitudes of these three positions were 30°W, 0° and 30°E, respectively. The southward displacement of the sea ice from these start sites was determined using the remote sensing products of ice velocity, instead of using buoy data as Lei et al. (2016). In comparison with buoy data, the advantage of the remote sensing product is temporal continuity. To reconstruct the ice trajectories, the daily positions of the sea ice were calculated from the successive drift vectors by applying the bilinear interpolation. When the sea ice reached a “no-data grid” that could not be approximated by interpolation, we treated the grid as a coastal region or as a marginal ice zone. Thus, the complete picture of the long-term changes of the southward displacement of sea ice in the Arctic outflow region could be obtained. To analyze the interannual change in the southward displacement of sea ice from the defined starting points toward the Fram Strait, we calculated the displacement beginning from 1 January every year.

The northward motion of the sea ice from the north of the NEP to the central Arctic might induce the formation of leads and polynyas along the NEP and accelerate the opening of the sea route. To compute the northward sea ice speed to the north of

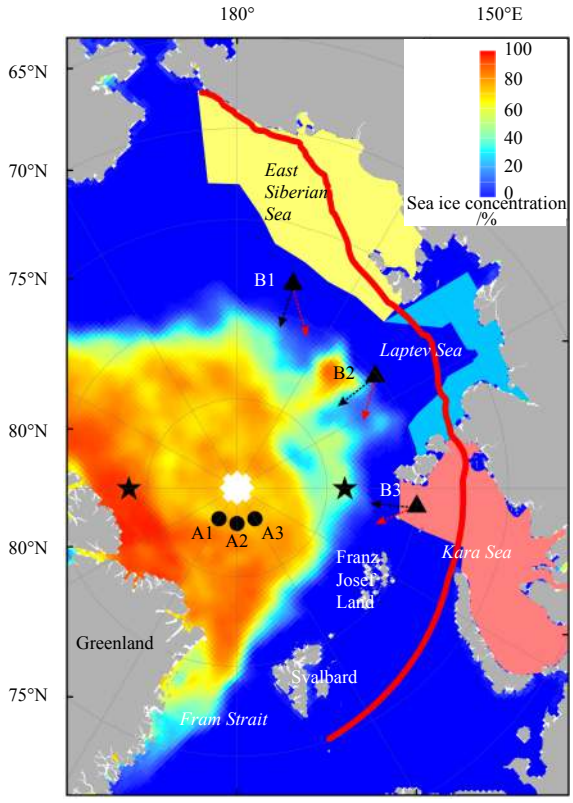

Fig. 1. Map of the central and eastern Arctic region with the monthly averaged sea ice concentration of September 2012. The red line denotes the defined Northeast Passage (NEP), polygons of different color denote the potential regions with polynyas along NEP, the black triangles and dots denote the test points to the north of the NEP and in the Arctic outflow region, and black stars mark the locations at which the sea level air pressures were used to calculate the CAI. The black and red arrows denote the direction north and a counterclockwise offset angle of 20° relative to north, respectively.

the NEP, we defined three fixed points: 78°N and 165°E (B1), 80°N and 130°E (B2), and 80°N and 85°E (B3) (black triangles in Fig. 1), corresponding to the sectors of the East Siberian Sea, Laptev Sea and Kara Sea, respectively.

2.2 *Evaluation of the NEP accessibility*

According to Lei et al. (2015), the track of the R/V *Xuelong* from the Chukchi Sea (68°N, 5°W) to the Norwegian Sea (75.1°N, 20°E) during summer 2012 was defined as the standard NEP (Fig. 1). As a region covered by sea ice with ice concentration less than 50% is considered safe for navigation for a Polar Class 6 icebreaker, such as the R/V *Xuelong*, we used this ice-concentration threshold to define the NEP open period. To obtain ice concentration information along the NEP, we calculated values for the test points at every 0.25° longitude along the sea route from June to November during 1979–2014 by using bilinear interpolation. The number of days with sea ice concentration lower than 50% was defined as the open period at the corresponding test point. To investigate the spatial variation of the open period along the sea route, we divided the NEP into three subsectors: the East Siberian, Laptev, Kara at 142°–179°E, 103°–142°E and 67°–103°E, respectively. A sea ice concentration product based on an algorithm of the National Aeronautics and Space Administration (NASA)-Team 2 was used to estimate the long-term changes in the open period for each of the NEP sectors. The ice concentration datasets were produced using passive microwave data from the Nimbus-7 Scanning Multichannel Microwave Radiometer (SMMR, 1979–1986), and Defense Meteorological Satellite Program (DMSP), Special Sensor Microwave/Imager (SSM/I, 1987–2007) and Special Sensor Microwave Imager Sounders (SMMIS, 2008 to present) available at ftp://sidads.colorado.edu/pub/DATASETS/.

2.3 *Atmospheric circulation pattern analysis*

To quantify the effect of the atmospheric circulation patterns on regulating sea ice kinematics within the TDS and to the north of the NEP, we calculated the monthly AO and DA indices, as well as the monthly CAI. The monthly SLP data of the National Centers for Environmental Prediction (NCEP) Reanalysis-2 north of 70°N were used to derive the empirical orthogonal function (EOF) modes, and the AO and DA were the first and second EOF modes (Wang et al., 2009). The CAI, defined as the difference in SLP between 84°N, 90°W and 84°N, 90°E (black stars in Fig. 1), was calculated using the ERA-Interim reanalysis data in accordance with Vihma et al. (2012). The regions defined by Preußer et al. (2016), which involved polynyas, were also considered to calculate the sea ice area in the months prior to the opening of the NEP (March–May) in the East Siberian, the Laptev Sea and the Kara Sea (Fig. 1). The sea ice area was calculated as the sum of the pixel areas with ice concentration over 15%, times the ice concentration (Parkinson et al., 1999).

An objective of this study was to clarify the relationship between sea ice kinematics to the north of the NEP and in the Arctic outflow region and the NEP accessibility. Therefore, we investigated the correlations between northward drift speed of sea ice to the north of the NEP and the NEP open period, and between the southward displacement of sea ice along the TDS and the NEP open period. Correlation analyses were also performed on the relationships between the northward drift (southward displacement) of the sea ice and the atmospheric circulation indices, and between the NEP open period and the atmospheric circulation indices, to quantify the response of the sea ice kinematics and of the NEP open period to the atmospheric circulation indices. The statistical significance of the correlation coefficients between the pairs of parameters was evaluated using the *t*-test.

3 Results

3.1 *Comparison of the data between ice motion products and drift buoys*

The correlation relationships and frequency distributions of the deviations between the ice drift speed derived from the buoy data and NSIDC and OSI SAF satellite-derived product from October 2011 to April 2012 are shown in Fig. 2. The NSIDC and OSI SAF products both demonstrated reasonably high correlation against the buoy data with the square of correlation coefficient (R^2) of 0.65 and 0.63, respectively. The frequency distributions of the deviations for both products were approximated as a normal distribution, but the deviations of the OSI SAF product had a wider range than the NSIDC product. The absolute value of the mode for the OSI SAF deviation (0.008 m/s) was smaller than that of the NSIDC deviation (0.009 m/s). The root mean square error (RMSE) was 0.05 m/s for the OSI SAF product, which was larger than that of the NSIDC product (0.04 m/s). These comparisons indicated that the NSIDC product had smaller scattering and lower error against the buoy data in comparison with the OSI SAF

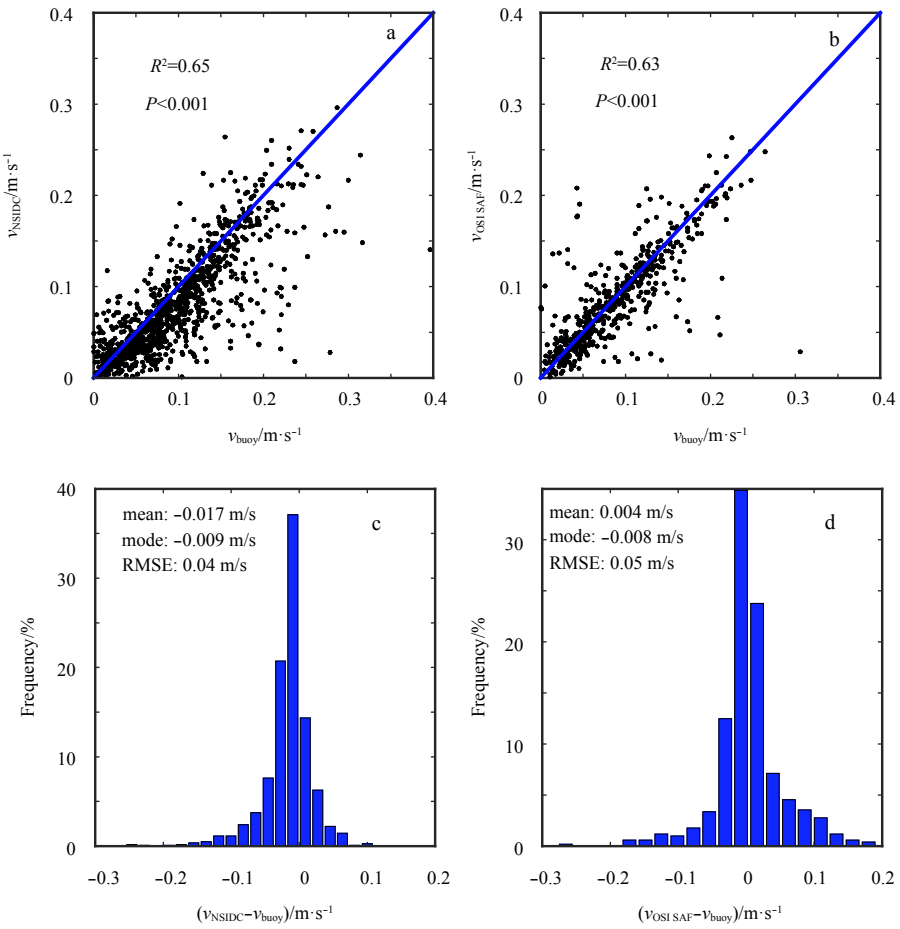

Fig. 2. Correlations between ice speeds (v) derived from the buoys and the sea ice motion products of NSIDC (a) and OSI SAF (b), and frequency distributions of the deviations against the buoy data of ice speed derived from the NSIDC (c) and OSI SAF products (d).

data. Considering its longer temporal coverage (1978 to present) and higher temporal resolution (daily), the NSIDC product was considered more suitable than the OSI SAF product to characterize the long-term changes in sea ice kinematics in the Arctic outflow region and to the north of the NEP.

3.2 *Changes of ice motion in the region to the north of the NEP and in the Arctic outflow region*

The monthly and annual northward sea ice speed derived for three fixed points from 1979 to 2014 was used to investigate the seasonal and long-term changes of the kinematic features of sea ice to the north of the NEP (Fig. 3). The northward drift speed decreased from January to early May and experienced an increase in B2 and B1 from May to August, but the variations of northward drift speed remained stable throughout the entire summer (JJA). The standard deviations (SDs) of the monthly northward sea ice speed in summer were relatively small in comparison with other seasons, and the lowest SDs were observed in August at all three sites. The continuous positive values of the northward component of ice speed at all the defined sites implied the summer sea ice dynamics to the north of the NEP contributed to the opening of the sea route. In summer, the northward drift speed of the Kara Sector was relatively weak in comparison with the other regions and in the other seasons. This indicated that ice advected offshore in summer was not the dominant factor causing the longer opening for this sector. The ice advected offshore in the freezing season would lead to the frequent breakup of sea ice and a thinner ice thickness prior to the summer melt season (Krumpen et al., 2013). This mechanism, associated with the heat advected from the Barents Sea led to the prolonged open period for this sector in comparison with those for the sectors of the Laptev Sea and East Siberian Sea.

An annual trend of increase of northward sea ice speed (+0.04 cm/s with P<0.05) from 1979 to 2014 was observed in the Kara sector in spring (Fig. 3b). The northward drift of the sea ice contributed to its thinning (Itkin and Krumpen, 2017), which resulted in the opening of sea route in spring. An annual trend of decrease of northward sea ice speed in summer of –0.03 cm/s (with P<0.05) is evident in Fig. 3c. This decreasing trend in summer observed in the Kara sector verified the northward drift of the ice to the north of the sea route in summer was not a leading factor governing the opening of the sea route at this sector. The annual average northward sea ice speed from 1979 to 2014 is shown in Fig. 3d. The significant trend of +0.02 cm/s (P<0.05) was only observed at B3, and the annually averaged northward drift speed was positive for all years. This indicates that the northward offshore ice advection was prevailing throughout the entire year for the Kara sector, which would lead to the ice thickness maintained at a lower level. This regulating pattern showed no exception for the years from 1979 to 2014.

From 1979 to 2014, increasing trends of southward sea ice displacement were found at all three sites (Fig. 4), and the R^2 values were 0.53 for 88°N and 30°W (A1), 0.50 for 88°N and 0° (A2), and 0.43 for 88°N and 30°E (A3), respectively. During 1979–2006, the

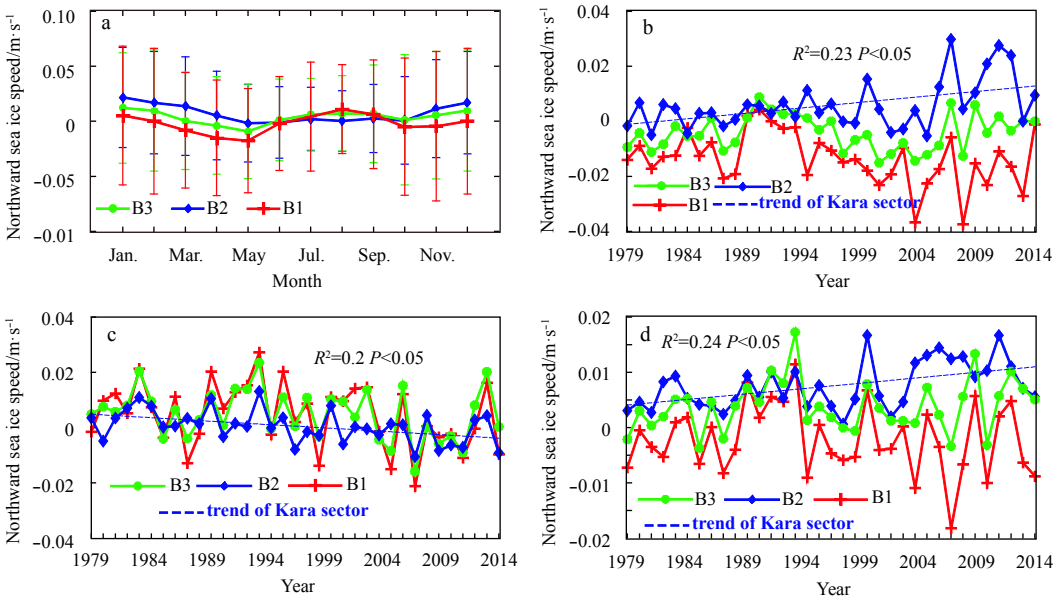

Fig. 3. Monthly variations (a) and long-term changes in spring (b), summer (c), and annual average (d) northward speed of sea ice at three fixed sites to the north of the NEP from 1979 to 2014. The significant trend was denoted by dashed line.

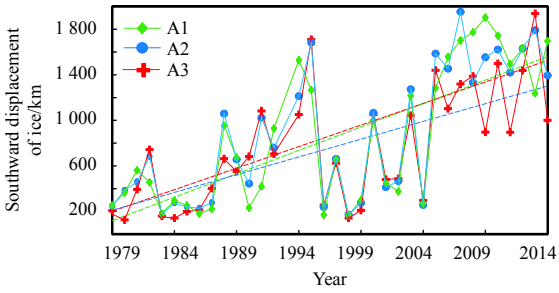

Fig. 4. Long-term variations of southward sea ice displacement from 88°N during 1979–2014. The dashed lines denote the trend at the 99.9% significance level.

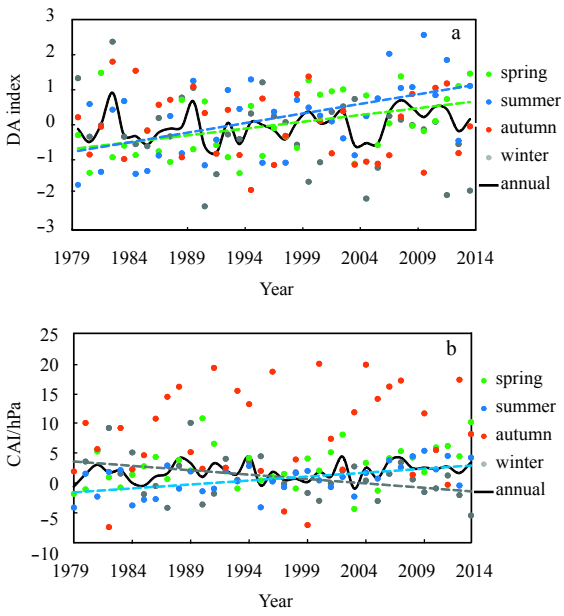

Fig. 5. Long-term changes in DA index (a) and CAI (b) from 1979 to 2014. The black solid lines denote the annual averages and the dashed lines the trends at the 95% significance level.

sea ice drifting from A2 and A3 reached the southernmost region in 1995, which was also observed by the ice drifting buoys (Lei et al., 2016). The fluctuations of southward displacement of the three sites were highly coherent from 1995 to 2005. However, in the recent decade (2005–2014), the southward sea ice displacements have shown spatial variation. The southernmost displacements of all three sites were observed after 2007, with the averages of 1 511 km in 2007–2014 more than twice those prior to 2007 (617 km). This large difference in variation might be attributed to that the mechanical connection among the ice pack in the Arctic outflow region became much weaker because of reduced ice thickness and decreased ice concentration.

To investigate the long-term changes of atmospheric circulation indices, the annual and seasonal averages of the DA index and CAI were calculated (Fig. 5). The annually averaged DA index varied dramatically but it did not show any significant trend. Seasonally, only the spring and summer DA indices (green and blue dashed lines in Fig. 5a) had significant increasing trends during the study period. A significantly increasing trend was found for the summer CAI (blue dashed line in Fig. 5b). The trends in summer for the DA index and CAI can partly explain the increasing trends of the southward displacements of sea ice drifting from the central Arctic Ocean.

3.3 *Changes in the NEP open period*

The spatially averaged open periods were calculated to investigate the long-term variations in the sectors of East Siberian, Laptev and Kara (Fig. 6a). Increasing trends at the 99.9% significance level were found in all three sectors with the R^2 of 0.39, 0.39 and 0.32 for the sectors of East Siberian, Laptev and Kara, respectively, which implied the enhanced accessibility for all these sectors during the study period. Here, we also investigated the correlation between the open period and the northward sea ice speed in spring, summer and autumn. However, only the northward sea ice speed in spring (March–May), which might be re-

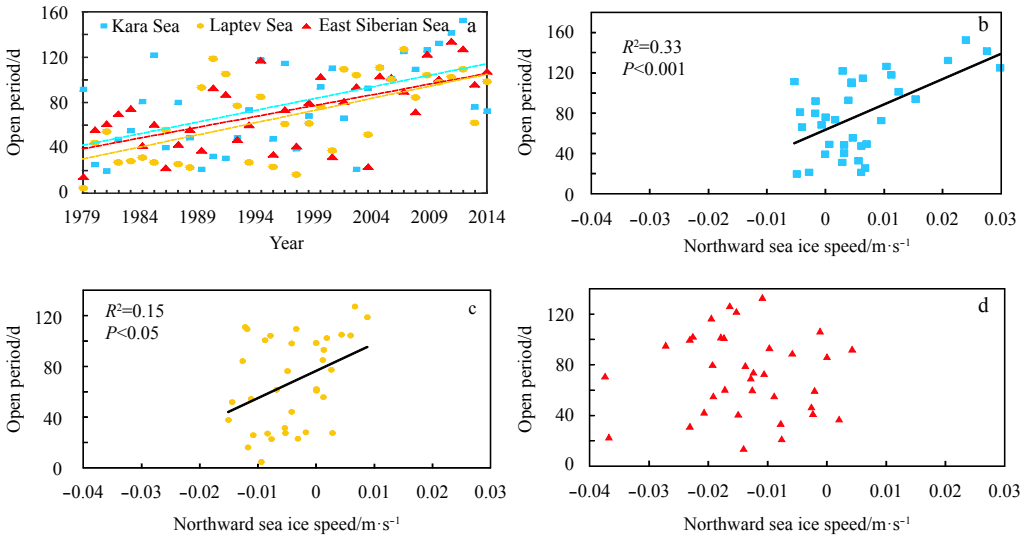

Fig. 6. Open period of three sectors along NEP from 1979 to 2014 (a), with the dashed lines denoting the long-term trends with 99.9% significance level, and the correlation relationships (b, c and d) of the spring (MAM) northward sea ice speed of the three fixed points to the north of the sea route and the open periods of the sea route for the sectors of Kara, Laptev, and East Siberian, respectively.

lated to the spring activities of coastal polynyas, had a statistically significant correlation with the open period in the sectors of Kara and Laptev (Fig. 6). Furthermore, no significant relationship was detected for the sector of East Siberian. This implied the opening of sea route in this sector was affected by other factors, for example, the thick multiyear ice advected from the western Arctic Ocean (Lei et al., 2015).

Correlation analyses were conducted between the average northward sea ice speed from March to May and sea ice area on 30 May of each year for the potential regions with polynyas as shown in Fig. 1 and between the sea ice area and the open period of the NEP (Fig. 7). A significant relationship was found between the northward sea ice speed and the sea ice area in the Kara and Laptev sectors. This can be explained as the northward sea ice

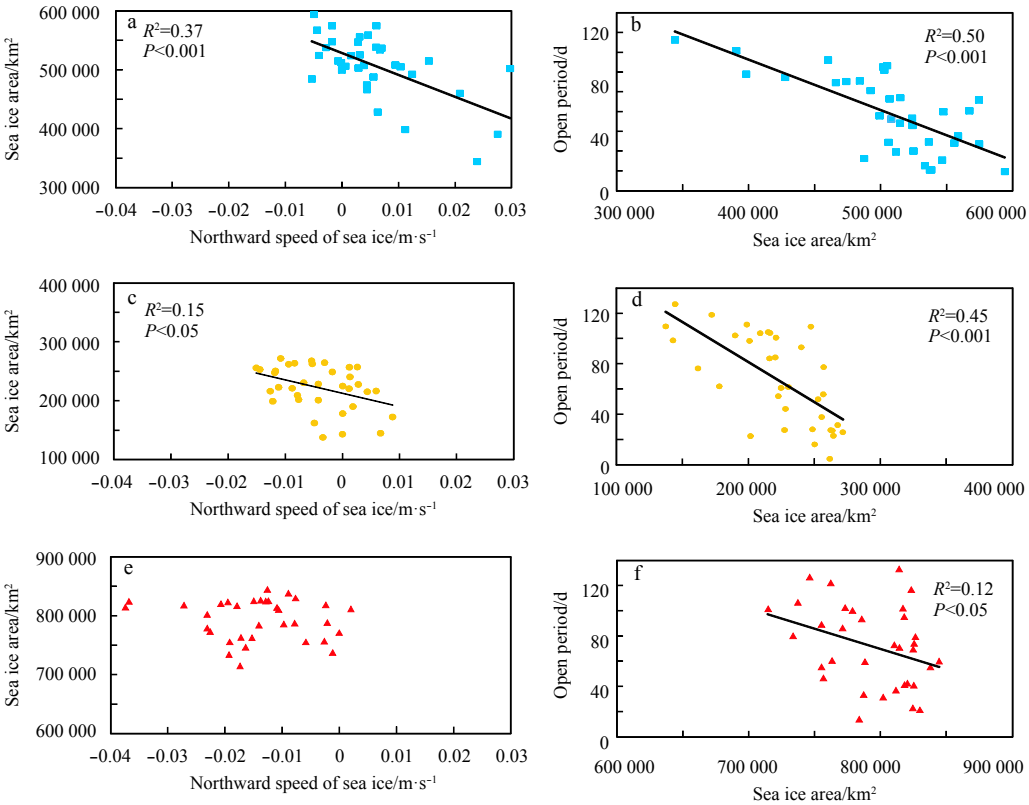

Fig. 7. Correlation between the average northward speed of sea ice to the north of the sea route from March to May and the sea ice area on 30 May in the potential region with polynyas for the sectors of Kara, Laptev, and East Siberian, respectively (a, c and e), and correlation between sea ice area in the potential region with polynyas and the open period for the different sectors (b, d and f).

drift contributing to the northward advection of sea ice, and it promoted the diminishment of sea ice area through the formation of leads and open water. Furthermore, the variation of sea ice area also had a significant relationship with the open period of these two sectors. To characterize the influence of the strength of the TDS on the accessibility of NEP, we evaluated the relationship between the average southward sea ice displacements from the three fixed points at 88°N from January to August and the NEP open period (Fig. 8). The open period in the East Siberian sector had the best correlation with southward sea ice displacement (R^2=0.47) followed by the Laptev sector (R^2=0.36), and the Kara sector (R^2=0.24). This could be explained as a reflection of the locations of the East Siberian and Laptev sectors were directly upstream of the TDS. Thus, the effect of the strength of the TDS on the opening of the sea route for these two sectors was more dominant than in the Kara sector.

3.4 *Responses of ice motion to atmospheric circulation indices*

As northward sea ice motion to the north of the NEP in spring was found to have a significant influence on the open period in the Kara and Laptev sectors, we evaluated the responses of northward sea ice speed in spring to the atmospheric circulation indices by applying the correlation analysis (Table 2). A significant relationship was found only for the CAI in the Laptev sector

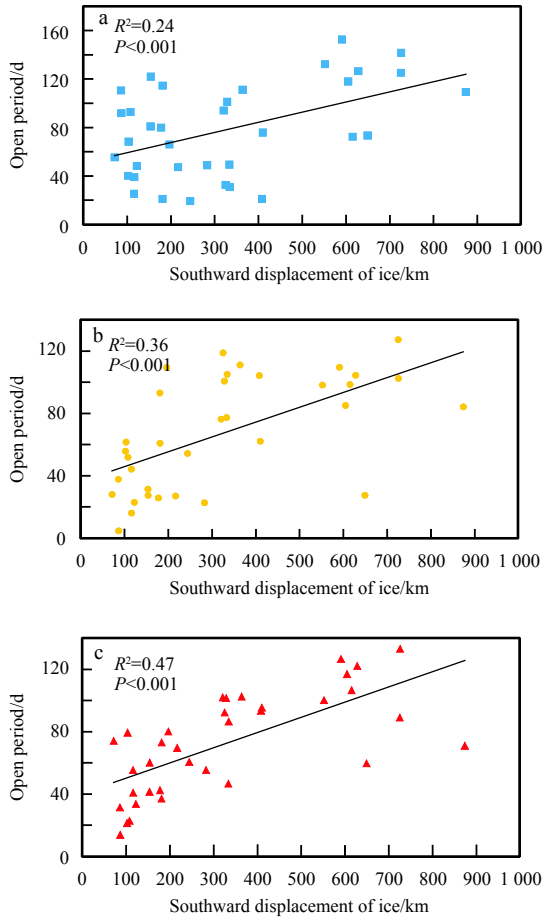

Fig. 8. Correlation relationships of the average southward sea ice displacement from three fixed points during 1 January to 31 August in the Arctic outflow region and the open periods of the sea route for the sectors of Kara (a), Laptev (b) and East Siberian (c), respectively.

Table 2. Statistical relationship between circulation indices with northward sea ice speed

	B1	B2	B3
CAI_sp vs. Northward speed of sea ice_sp	n.s.	0.14*	n.s.
DA_sp vs. Northward speed of sea ice_sp	n.s.	n.s.	n.s.

Note: Significance level is P<0.05 (*); n.s. denotes not significant at the 0.05 significance level. Subscripts sp denote spring (March to May).

with R^2 of 0.14. However, no significant correlation between the DA index and northward sea ice speed was observed in any sectors. As for the responses of sea ice motion to the atmospheric circulation indices, generally, wind oriented to the line connecting the high- and low- centers of SLP would have a strong coherence with the difference of the SLP between the centers (Kwok, 2000). In the central Arctic Ocean, the angle of deviation between ice drift and wind heading is about 20° (Lei et al., 2016). As shown in Fig. 1, the heading of the wind force related to the northward ice speed to the north of the Kara sector (red arrow) was almost parallel to the line connecting the high- and low- centers of the CAI. Thus, the relationship between ice drift to the north of Kara sector and the CAI was found insignificant. Both the distance between the defined site and the line connecting the high- and low- centers and the intersection angle between the heading of wind and the connecting line were greater for the sector of East Siberian than for the sector of Laptev. Thus, the relationship between sea ice drift speed to the north of East Siberian sector and the CAI was found weaker than for the Laptev sector. The uncertainty of the locations of the high- and low- centers of DA resulted in a weaker relationship with the northward sea ice speed to the north of the sea route compared with that for the CAI.

The responses of the TDS to the circulation indices were analyzed by applying correlation analyses between the southward sea ice displacement starting from 88°N from January to August and the average CAI and DA index in spring-summer (Fig. 9). Both the CAI and DA index showed significant relationships with the southward sea ice displacement at all sites. Regression analyses showed that DA index and CAI could explain the variations of southward sea ice displacement by 45%, and 45.2%, respectively. Furthermore, the sea ice drift trajectories were reconstructed to investigate the southward sea ice drift in spring-summer under extreme conditions (Fig. 10). It was found that the sea ice could have traveled furthest south in 2014 and 2012 with extremely high positive spring-summer CAI (1 697 km) and DA index (1 069 km), respectively. By the end of August, the floes were advected southward to 72.8°–80°N under this condition, with the net southward displacements of 893–1 697 km. On the contrary, the floes were restricted to the central Arctic region when the spring-summer CAI and DA index were extremely low in 2004 (277 km) and 1984 (123 km). By the end of August, the floes were advected southward to 85.3°–86.9°N in these two years, with the net southward displacements of 123–302 km. Notably, the sea ice tended to drift toward the north of Greenland in the years with an extremely low CAI, which can be attributed to the weaker geostrophic wind associated with a low CAI (Vihma et al., 2012).

The correlation analyses between circulation indices in spring-summer and southward sea ice displacement revealed that both CAI and DA had a significant influence on the sea ice export towards the Fram Strait. Moreover, the net southward displacement from 88°N during 1 January to 31 May and 1 June to 31 August were calculated to represent the southward sea ice displacement in spring and summer, respectively, and the seasonal

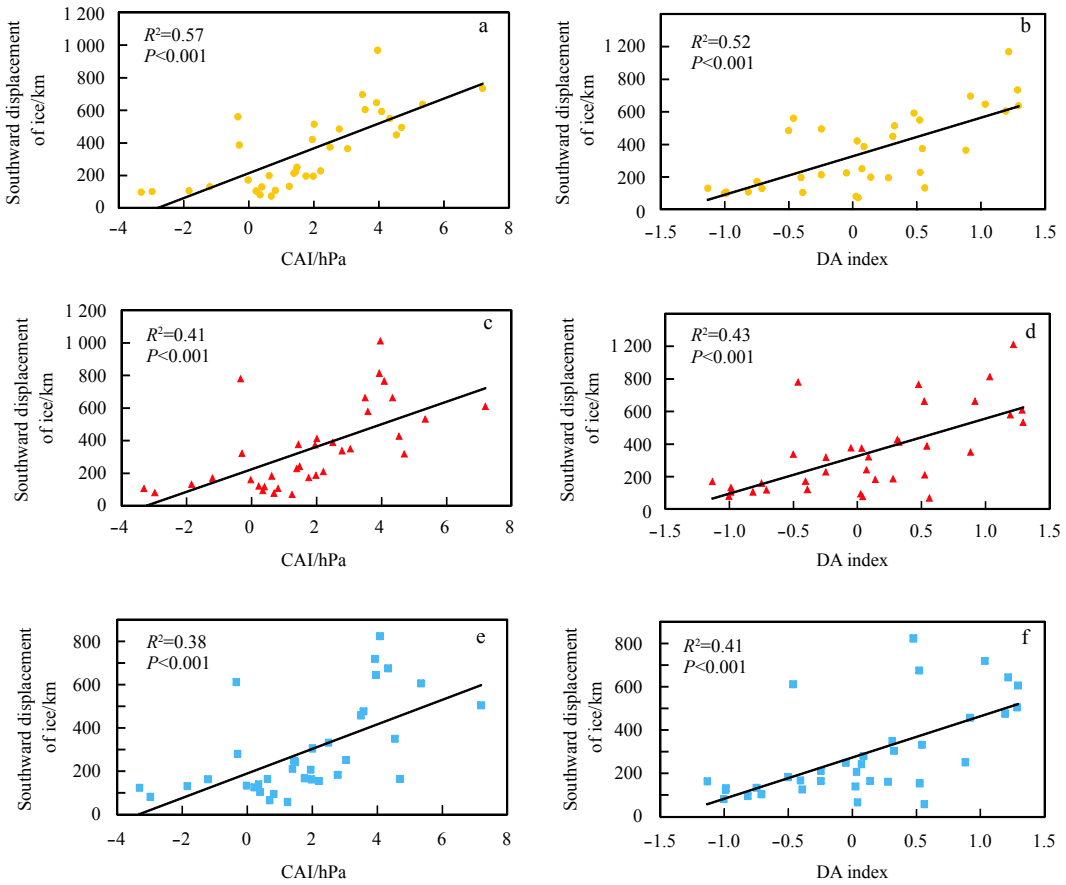

Fig. 9. Correlation between spring-summer averaged CAI (a, c and e) or DA index (b, d and f) and the southward displacements from the three fixed points at 88°N from 1 January to 31 August. The orange dots, red triangles and blue squares denote the displacements starting from A3, A2 and A1, respectively.

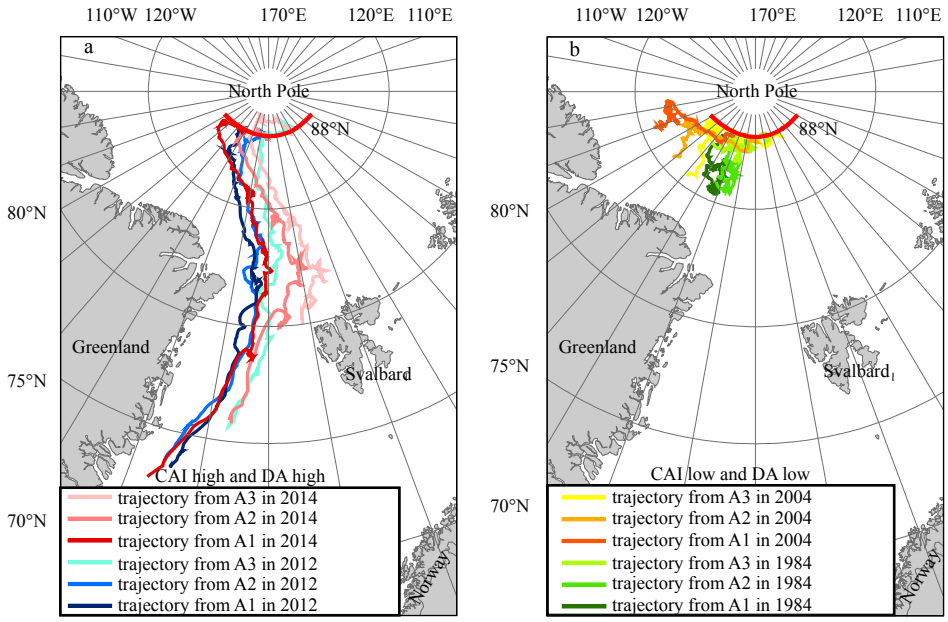

Fig. 10. Trajectories of sea ice drift from 88°N in spring-summer with high DA index and CAI (a), and low DA index and CAI (b).

correlation was also examined to quantify the influential mechanism (Table 3). The spring CAI and DA could better explain the southward sea ice displacement compared with those calculated until the end of summer, and spring CAI had higher correlation coefficient and significance level than those for spring DA at the same sites.

Table 3. Statistical relationship between circulation indices with southward sea ice displacement

	A3	A2	A1
CAI_sp vs. Southwards ice displacement_sp	0.42***	0.24**	n.s.
CAI_su vs. Southwards ice displacement_su	0.20**	0.14*	n.s.
DA_sp vs. Southwards ice displacement_sp	0.25**	0.14*	0.12*
DA_su vs. Southwards ice displacement_su	0.21**	0.15*	n.s.

Note: Significance levels are $P<0.001$ (***), $P<0.01$ (**) and $P<0.05$ (*); n.s. denotes not significant at the 0.05 significance level; and sp and su spring (March to May) and summer (June to August), respectively.

3.5 *Responses of the NEP open period to atmospheric circulation indices*

According to the results of the correlation analyses between the northward sea ice speed to the north of NEP and the NEP open period, and between the circulation indices and northward sea ice speed, only the spring northward sea ice drift related to the CAI could explain the variation of the open period in the Laptev sector. However, it was found that the atmospheric circulation indices could be related to the NEP open period via other mechanisms because the significant correlations were observed (Table 4). The spring and summer CAI had significant associations with the open period in the East Siberian and the Laptev sectors. In particular, correlation coefficients of the spring CAI in these two sectors exceeded 0.5 at the 99.9% significance level. The summer CAI had a greater correlation for the Laptev sector (R^2=0.42) than East Siberian sector (R^2=0.28), but no significant correlation was detected in Kara sector. The spring DA index only had significant correlation with the open period in the Laptev sector with the R^2 of 0.22. While the summer DA index demonstrated significant correlation in all sectors. Moreover, the square of correlation coefficient in the Laptev sector (R^2=0.31) was greater than for both the East Siberian sector (R^2=0.30) and Kara sector (R^2=0.21). The trend of increase of the summer DA index from 1979 to 2014 would increase the export of sea ice out of the Arctic Basin through the Fram Strait. Thus, the thinner and weaker sea ice in the East Siberian, Laptev, and Kara sectors would be dispersed more easily under the influence of the summer DA, which would strengthen the accessibility of the sea route.

4 Discussion

The OSI SAF and NSIDC sea ice motion products are used widely for models validation and data assimilation. The errors of such products have been evaluated by comparison with drifting buoys (Lavergne et al., 2010) and by intercomparison of the products (Hwang, 2013). The reasonably small uncertainties of the NSIDC product found in this study were consistent with the findings of Sumata et al. (2014). The sea ice kinematics characterized as the southward sea ice displacement in the Arctic outflow region indicated the ability of the TDS to export sea ice from the central Arctic to Fram Strait. Haller et al. (2014) found that the TDS in 2007–2009 was twice as fast as the drift of Vessel Fram, and our findings verified enhancement of the TDS since 2007. This could also explain the rapid loss of Arctic sea ice in recent years from the dynamic perspective. However, this rapid outflow of Arctic sea ice cannot be defined as a new normal because such a state was also observed in 1994–1995.

Table 4. Statistical relationships between circulation indices and the open periods

	East Siberian sector	Laptev sector	Kara sector
CAI_sp vs. open period	0.37***	0.29***	n.s.
CAI_su vs. open period	0.28**	0.42***	n.s.
DA_sp vs. open period	n.s.	0.22**	n.s.
DA_su vs. open period	0.30***	0.31***	0.21**

Note: Significance levels are $P<0.001$ (***) and $P<0.01$ (**); n.s. denotes not significant at the 0.05 significance level; and sp and su spring (March to May) and summer (June to August), respectively.

The northward sea ice speed was proven to be a good indicator of sea ice kinematic characteristics to the north of NEP. However, not all the defined sites exhibited strong relationships with the NEP open period, which might account for the limitation of analysis based on the defined points set to the north of the NEP. Additional auxiliary data, e.g., the wind forcing, will be required to explore the detail of the relationship in further study. The diminishment of the sea ice area in spring, which contributed to the NEP opening, might have connections with polynya activities along the NEP. Our results showed significant relationship between sea ice area and open period in the sectors of Kara, Laptev and East Siberian. As these sectors are dominated by several polynyas, we considered that the polynya activity affected the sea ice area of these regions, which ultimately influenced the NEP open period. This inference has been supported by previous work by Bareiss and Görgen (2005), who suggested that increasing polynya activities in spring could lead to an increase in the open-water area from summer to early fall, which indicated an extension of the melt period. However, the accurate locations and extent of polynyas have not been quantified from the observational data in the current work. The direct relationship between polynya activity and the NEP open period in these sectors could be explored further in the future.

5 Conclusions

The NSIDC product of sea ice motion was applied to reconstruct the northward speed of sea ice to obtain the kinematic features of the sea ice to the north of NEP. The strength of the TDS was also evaluated based on the southward displacement of sea ice in the Arctic outflow region. In the regions to the north of the NEP, the long-term trend of averaged northward sea ice speed in the Kara sector was +0.04 cm/s per year in spring and –0.03 cm/s per year in summer, while no significant long-term trends were observed in the other sectors or in the other seasons. In the Arctic outflow region, a trend of increase of the annually averaged southward sea ice displacement was found for all fixed points in 88°N over our study period. The average southward displacement in 2007–2014 (1 511 km) was more than twice the average prior to 2007 (617 km), which indicated continuous enhancement of the TDS in comparison with previous years.

The increasing trend of the NEP open period was found in the East Siberian, Laptev, and Kara sectors. The northward sea ice speed in spring could explain the variation of opening sea route by 33% and 15% in the Kara and Laptev sectors, respectively. The response of the NEP open period to the southward sea ice displacement along the TDS was significant in the East Siberian and Laptev sectors in comparison with the Kara sector. As a simple index for quantifying the pressure gradient across the TDS, the CAI has significant impacts on both the opening of the sea route

along the NEP and the export of sea ice toward the Fram Strait. Based on the correlation analyses between the circulation indices and the open period, we conclude that offshore sea ice advection in spring contributes to the early opening of the sea routes and preconditions the melt processes in summer.

References

Bareiss J, Görgen K. 2005. Spatial and temporal variability of sea ice in the Laptev Sea: analyses and review of satellite passive-microwave data and model results, 1979 to 2002. Global and Planetary Change, 48(1–3): 28–54, doi: 10.1016/j.gloplacha.2004.12.004

Cavalieri D J, Parkinson C L, Gloersen P, et al. 1996. Sea ice concentrations from nimbus-7 SMMR and DMSP SSM/I-SSMIS passive microwave data, version 1. Boulder, Colorado USA: NASA DAAC at the National Snow and Ice Data Center

Comiso J C, Hall D K. 2014. Climate trends in the Arctic as observed from space. Wiley Interdisciplinary Reviews: Climate Change, 5(3): 389–409, doi: 10.1002/wcc.277

Dmitrenko I, Kirillov S, Eicken H, et al. 2005. Wind-driven summer surface hydrography of the eastern Siberian shelf. Geophysical Research Letters, 32(14): L14613

Dmitrenko I A, Kirillov S A, Tremblay L B. 2008. The long-term and interannual variability of summer fresh water storage over the eastern Siberian shelf: implication for climatic change. Journal of Geophysical Research, 113(C3): C03007

Dmitrenko I A, Kirillov S A, Tremblay L B, et al. 2009. Sea-ice production over the Laptev Sea shelf inferred from historical summer-to-winter hydrographic observations of 1960s–1990s. Geophysical Research Letters, 36(13): L13605, doi: 10.1029/2009GL038775

Haller M, Brümmer B, Müller G. 2014. Atmosphere-ice forcing in the transpolar drift stream: results from the DAMOCLES ice-buoy campaigns 2007–2009. The Cryosphere, 8(1): 275–288, doi: 10.5194/tc-8-275-2014

Hurrell J W. 1995. Decadal trends in the North Atlantic Oscillation: regional temperatures and precipitation. Science, 269(5224): 676–679, doi: 10.1126/science.269.5224.676

Hwang B. 2013. Inter-comparison of satellite sea ice motion with drifting buoy data. International Journal of Remote Sensing, 34(24): 8741–8763, doi: 10.1080/01431161.2013.848309

Itkin P, Krumpen T. 2017. Winter sea ice export from the Laptev Sea preconditions the local summer sea ice cover and fast ice decay. The Cryosphere, 11(5): 2383–2391, doi: 10.5194/tc-11-2383-2017

Krumpen T, Janout M, Hodges K I, et al. 2013. Variability and trends in Laptev Sea ice outflow between 1992–2011. The Cryosphere, 7(1): 349–363, doi: 10.5194/tc-7-349-2013

Kwok R. 2000. Recent changes in Arctic Ocean sea ice motion associated with the North Atlantic Oscillation. Geophysical Research Letters, 27(6): 775–778, doi: 10.1029/1999GL002382

Kwok R, Rothrock D A. 1999. Variability of fram strait ice flux and North Atlantic Oscillation. Journal of Geophysical Research, 104(C3): 5177–5189, doi: 10.1029/1998JC900103

Kwok R, Spreen G, Pang S. 2013. Arctic sea ice circulation and drift speed: decadal trends and ocean currents. Journal of Geophysical Research, 118(5): 2408–2425

Lasserre F, Pelletier S. 2011. Polar super seaways? Maritime transport in the Arctic: an analysis of shipowners' intentions. Journal of Transport Geography, 19(6): 1465–1473, doi: 10.1016/j.jtrangeo.2011.08.006

Lavergne T, Eastwood S, Teffah Z, et al. 2010. Sea ice motion from low-resolution satellite sensors: an alternative method and its validation in the Arctic. Journal of Geophysical Research, 115(C10): C10032, doi: 10.1029/2009JC005958

Lei Ruibo, Heil P, Wang Jia, et al. 2016. Characterization of sea-ice kinematic in the Arctic outflow region using buoy data. Polar Research, 35(1): 22658, doi: 10.3402/polar.v35.22658

Lei Ruibo, Xie Hongjie, Wang Jia, et al. 2015. Changes in sea ice conditions along the Arctic Northeast Passage from 1979 to 2012. Cold Regions Science and Technology, 119: 132–144, doi: 10.1016/j.coldregions.2015.08.004

Lindsay R, Schweiger A. 2015. Arctic Sea ice thickness loss determined using subsurface, aircraft, and satellite observations. The Cryosphere, 9(1): 269–283, doi: 10.5194/tc-9-269-2015

Nghiem S V, Rigor I G, Perovich D K, et al. 2007. Rapid reduction of Arctic perennial sea ice. Geophysical Research Letters, 34(19): L19504, doi: 10.1029/2007GL031138

Parkinson C L, Cavalieri D J, Gloersen P, et al. 1999. Arctic sea ice extents, areas, and trends, 1978–1996. Journal of Geophysical Research, 104(C9): 20837–20856, doi: 10.1029/1999JC900082

Preußer A, Heinemann G, Willmes S, et al. 2016. Circumpolar polynya regions and ice production in the Arctic: results from MODIS thermal infrared imagery from 2002/2003 to 2014/2015 with a regional focus on the Laptev Sea. The Cryosphere, 10(6): 3021–3042, doi: 10.5194/tc-10-3021-2016

Rigor I G, Wallace J M, Colony R L. 2002. Response of sea ice to the Arctic Oscillation. Journal of Climate, 15(18): 2648–2663, doi: 10.1175/1520-0442(2002)015<2648:ROSITT>2.0.CO;2

Spreen G, Kwok R, Menemenlis D. 2011. Trends in Arctic sea ice drift and role of wind forcing: 1992-2009. Geophysical Research Letters, 38(19): L19501

Sumata H, Lavergne T, Girard-Ardhuin F, et al. 2014. An intercomparison of Arctic ice drift products to deduce uncertainty estimates. Journal of Geophysical Research, 119(8): 4887–4921

Thompson D W J, Wallace J M. 1998. The Arctic oscillation signature in the wintertime geopotential height and temperature fields. Geophysical Research Letters, 25(9): 1297–1300, doi: 10.1029/98GL00950

Tschudi M, Fowler C, Meier W. 2016. Polar pathfinder daily 25 km EASE-Grid sea ice motion vectors, version 3. Boulder, Colorado USA: NASA National Snow and Ice Data Center Distributed Active Archive Center

Vihma T, Tisler P, Uotila P. 2012. Atmospheric forcing on the drift of Arctic sea ice in 1989–2009. Geophysical Research Letters, 39(2): L02501

Wang Jia, Ikeda M. 2000. Arctic oscillation and Arctic sea-ice oscillation. Geophysical Research Letters, 27(9): 1287–1290, doi: 10.1029/1999GL002389

Wang Jia, Zhang Jinlun, Watanabe E, et al. 2009. Is the Dipole Anomaly a major driver to record lows in Arctic summer sea ice extent?. Geophysical Research Letters, 36(5): L05706

Wu Bingyi, Wang Jia, Walsh J E. 2006. Dipole anomaly in the winter arctic atmosphere and its association with Sea Ice Motion. Journal of Climate, 19(2): 210–225, doi: 10.1175/JCLI3619.1

Zhang Xiangdong, Ikeda M, Walsh J E. 2003. Arctic sea ice and freshwater changes driven by the atmospheric leading mode in a coupled sea ice-ocean model. Journal of Climate, 16(13): 2159–2177, doi: 10.1175/2758.1